Electronic Supplementary Material (ESI) for Soft Matter.

Supporting Information

Membranes under shear stress: visualization of non-equilibrium domain patterns and domain fusion in a microfluidic device

Flurin Sturzenegger[1‡], Tom Robinson[1‡], David Hess[1], Petra S. Dittrich[1,2] *

ETH Zurich, Switzerland, [1]Department of Chemistry and Applied Biosciences, [2]Department of Biosystems Science and Engineering

List of movies.

The movies show vesicles, where the l_d phase, stained with DiI, is visualized.

Movie 1 shows a surface-tethered giant unilamellar vesicle that is subjected to flow. Tracer particles are used to visualize the flow. In **movie 2**, the flow is finally stopped.

Movie 3 shows the immediate stop of the flow inside the chamber when the valve is closed. Fluorescent beads are used as tracer particles.

Movie 4 depicts a trapped vesicle with fusing domains after stopping the flow, corresponding to figure 2.

Movie 5 depicts a trapped vesicle, where domains are not fusing after stopping the flow, corresponding to figure 3.

Movie 6 depicts a trapped vesicle after stopping the flow at elevated temperature of T=37 °C, corresponding to figure 4.

Movie 7 depicts a trapped vesicle with the composition of SM/DOPC/Chol 0.52:0.22:0.26 which has not been exposed to flow.

Content list

1. Materials and Methods.

Chemicals. All chemicals were used as received without further purification. Sphingomyelin (egg chicken, SM), 1,2-Dioleoyl-*sn*-glycero-3-phosphocholine (DOPC) and cholesterol were purchased from Avanti Polar Lipids. The fluorophore 1,1'-Dioctadecyl-3,3,3',3'-Tetramethylindocarbocyanine Perchlorate (DiI) was from Life Technologies, Naphtho[2,3-a]pyrene (NAP) from TCI Deutschland GmbH, bovine serum albumin (BSA) was from Sigma Aldrich, ethanol from Scharlau (Spain), methanol and chloroform from Acros Organics (Switzerland), sodium hydroxide (NaOH) from Merck Schuchardt OHG (Germany). Poly(dimethylsiloxane)(PDMS) was ordered from Dow Corning (trade name Sylgard 184).

Vesicle preparation. Giant unilamellar vesicles were formed by electroformation[1] using ITO coated glass slides (Sigma Aldrich, 15-25 Ω/sq, 26 X 75 X 0.5 mm) which were first cleaned by sonication for 30 min in NaOH and for 30 min in Ethanol. They were then heated at 100 °C for 5 min to fuse any cracks in the ITO layer.[2] A home-made chamber device was used which contained a silicone rubber spacer to separate the two ITO-slides with twelve holes, which formed twelve separate growing chambers. Copper contacts were used in between the rubber and the ITO slides to connect them to an arbitrary function generator (Hameg instruments, HMF 2525). 10 µl of the lipid solution was pipetted in each well. To completely remove all solvent, the slide was placed in the desiccator over night at 100 mbar. Then the lipids were rehydrated with 175 µL Millipore water in each well and the top ITO-slide was added. The lipids had to be heated above the melting temperature during the electroformation, which was achieved with a home-made heating block equipped with a temperature sensor. The lipids were first heated to 60 °C and then an alternating current of 1 V and 10Hz was applied for 2.5 hours to form the GUVs. Then the device was cooled down to room temperature and a current of 1.5 V and 3 Hz was applied for half an hour to detach all the GUVs from the lipid film. The top ITO slide was carefully removed and the GUV solution harvested with a pipette. Two types of GUVs were used with the compositions of SM/DOPC/Chol in 0.52:0.22:0.26 molar ratios and 0.4:0.4:0.2, with average Ld/(Lo+Ld) area fraction ratios of 0.37 and 0.15, respectively. To these mixtures, the dye solutions (DiI and NAP) were added to a final concentration of 0.1 mol%.

Microfluidic device operation. For the initial experiments we used a microfluidic chip made of PDMS and covered by a glass slide. It had one straight channel of different dimensions, with a height of 20 µm, and the GUV immobilization protocol that was previously described.[3] Due to the GUV rotation and fast detachment, we developed a microfluidic chip with an array of taps surrounded by round valves that can be actuated to immediately stop the flow. The design and fabrication is described in a former work.[4] For this work, the heights of the microfluidic channels were 30 µm, if not indicated otherwise. A photograph and the scheme of the microchannels are given in the Figure S1.

After assembling the chip, the channels were coated with albumin by incubating them for 30 min with a 0.04 g/ml solution of BSA in water. To initially fill the channels, the fluids were centrifuged into the channels at a relative centrifugal force of 950 for 10 min. Because PDMS is gas permeable, all the air in the chip was pressed out during centrifugation. After the initial filling, the flow in the fluid layer was controlled by suction using a pump (neMESYS, Cetoni, Germany) and a 1 mL glass syringe (Agilent). To control the pressure layer, i.e. actuating the valves, a custom built control-box was used. It had eight different outlets, which could be individually switched on or off. The outlets were connected to the eight chip inlets with tubing and custom metal connectors. To lower the valves a pressure of 3.5 bar was required. To remove the BSA solution, the chip was first flushed with 90 µl water at a flow rate of 15 µL/min. Then the chip was loaded with the GUV solution at a flow rate of 7.5 µL/min.

After trapping the GUVs, the valves were closed and surplus GUVs were washed out. At open valves the trapped GUVs were subjected to flow rates of up to 40 µL/min.

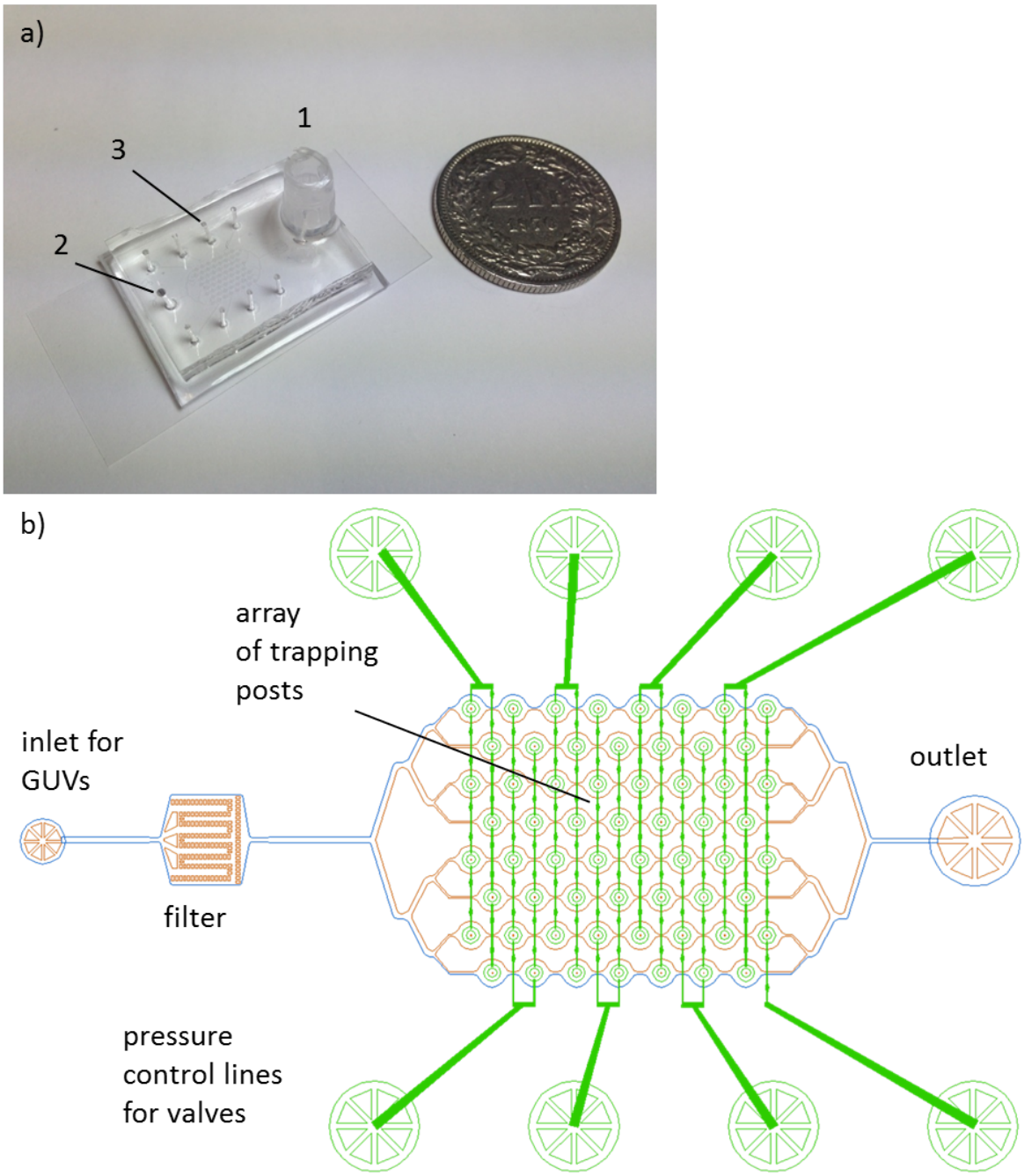

Figure S1. *a) Photograph of the final chip, with inlet (1), outlet (2) and pressure control connections (3). A two Franc coin is given for scale. b) Schematics of the fluid channels in red/blue, and the pressure control lines in green.*

Optical microscopy. GUVs were observed on a Zeiss 200M (inverse) microscope, equipped with an EMBL incubator box GP 168. Two objectives were used: A 10x 0.3NA Plan-Neofluar and a 63x 1.4NA Oil Plan-Apochromat (Zeiss). The fluorophore NAP was excited by an Argon laser at 458 nm and fluorescence was detected using a band-pass filter (500-550 nm). For the fluorophore DiI a solid state laser (561nm) was used and a long-pass filter (575

nm). Scanning parameters such as pinhole size, laser intensity, image resolution or scanning speed were adjusted for each measurement, to get a good balance between image quality and acquisition speed. For image processing and analysis, the software ImageJ was used.

2. Non-equilibrium domain patterns

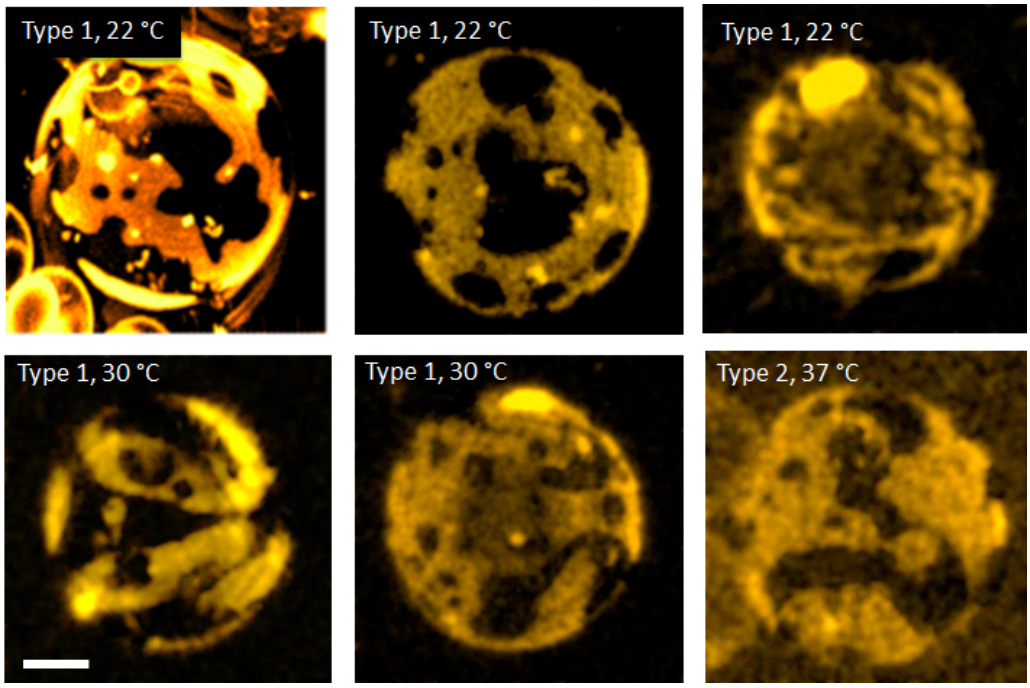

Figure S2. *Transient patterns of domains taken in the moment when the flow was stopped using a microfluidic device with a simple straight channel. The large boundary between liquid ordered and disordered phases (orange, stained with DiI) are clearly visible. As the acquisition time per image takes several hundred ms per image, rotation or movements of the vesicle may partially result in stretching of domains. GUV types 1 and 2 refer to the composition SM/DOPC/Chol in 0.52:0.22:0.2 molar ratios and 0.4:0.4:0.2, respectively. Temperatures are as indicated. Scale bar: 10 µm. Brightness and contrast of the images were increased to improve the visualization of the phases.*

3. Analysis of individual domains after the application of shear stress

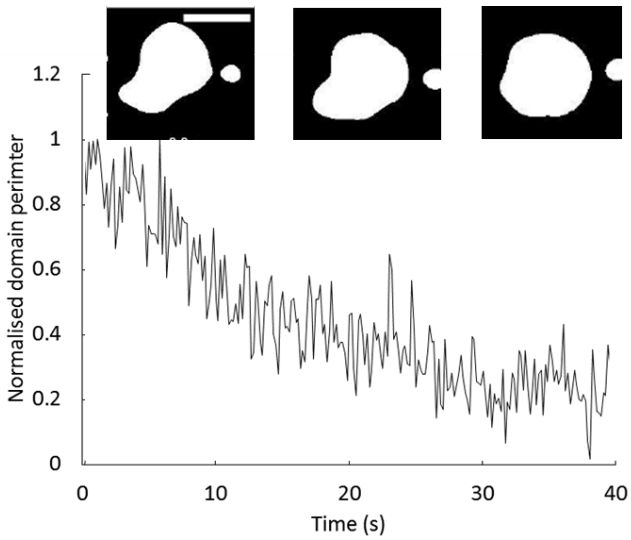

Figure S3. *Image analysis of a domain after flow has been arrested. ImageJ was used to create binary images, which were then analyzed for interface perimeter. Inserts are at 0, 20, and 40 s after flow was stopped. This single domain reaches a minimum boundary state in approximately 30-40 s. Scale bar: 5 µm.*

4. **Performance of ring-shaped valves**

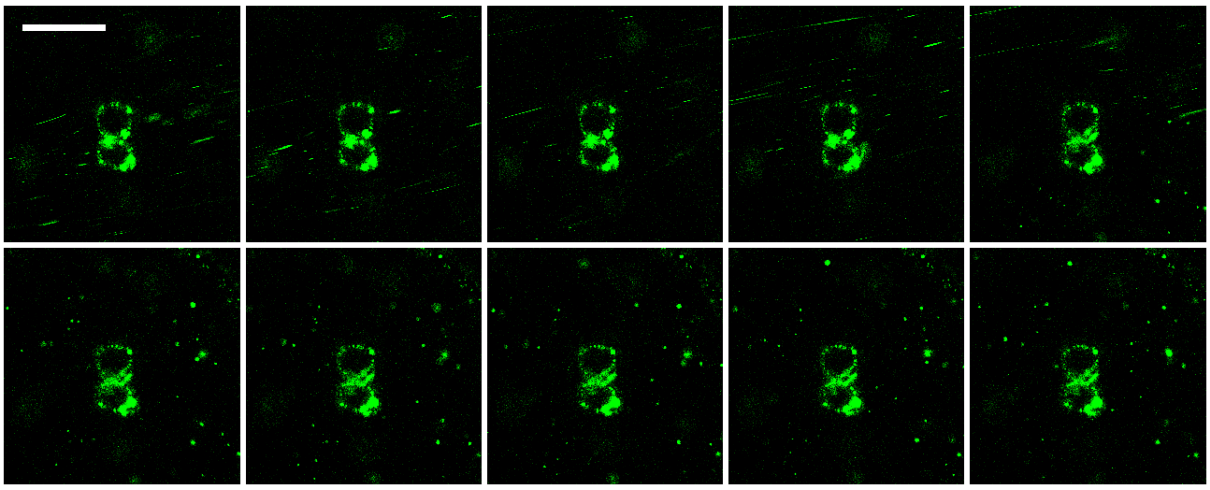

Figure S4. *Time series of fluorescent beads being stopped by a valve. In the middle of the images, beads can be seen that are unspecifically binding to the PDMS traps. The ring valve is lowered during acquisition of panel five and the flow is immediately stopped. Scale bar: 50 µm. See also movie 3.*

5. Deformation of GUVs in flow

To show how fast GUVs return to a spherical shape after stopping shear stress, we measured different sized GUVs at different flow rates and stopped the flow by lowering the valve. Time series of a slice in the middle of the GUV were collected and the diameters in x- and y-

direction (D_x and D_y respectively) of the shape were measured before, during and after closing the valve. In Fig.S7 such a time series is shown. It can be seen that the GUV returns to a spherical shape within one frame and doesn't change thereafter.

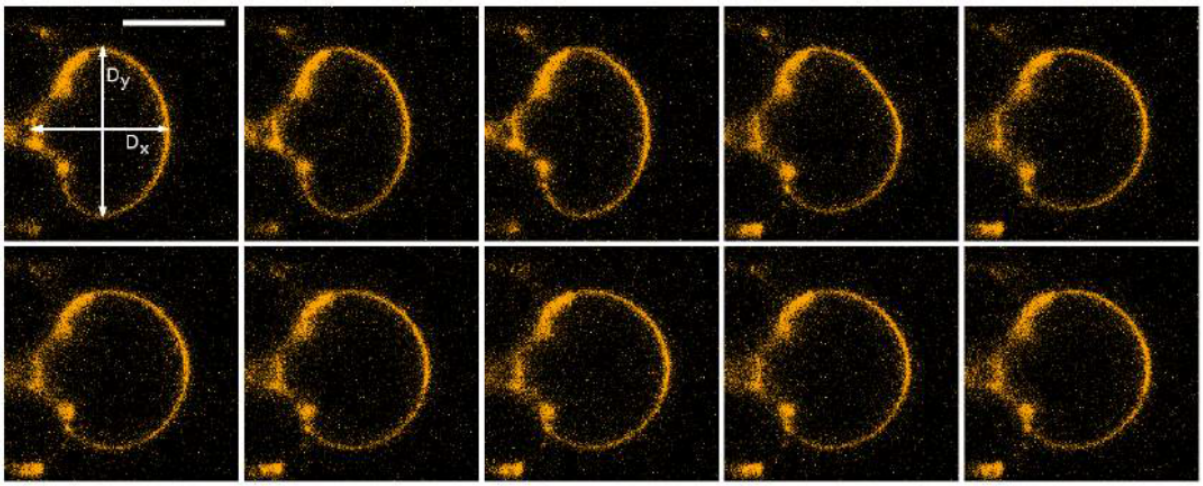

Figure S5: *GUV being compressed with a flow of 40 µL/min (DiI channel). During panel four the valve is lowered. The images are taken at intervals of 0.3 s. In the first panel the measured D_x and D_y are indicated. Scale bar: 20 µm.*

In this example it can be seen that the GUV appears to be stuck in the trap even after the flow is stopped. This would be a problem when measuring domain movement, because one phase might prefer the bent part of the membrane, restricting its movement. In most cases however, the GUVs wouldn't interact with the traps after the flow was stopped. When measuring GUVs with domains, only the cases without interactions with the traps were evaluated. In Fig.S8 plots of D_x and D_y of three different sized GUVs are shown. They were each compressed with 10, 20, 30 and 40 µL/min flows. One would expect that D_x is smaller than D_y during shear stress, because the GUV is compressed. When the flow is stopped, D_x should rise and D_y should decline until the GUV is circular and D_x and D_y have the same length.
For the smallest GUV (12.5 µm) not much change in shape can be observed when closing the valve (at around 0.8 s). This means that the GUV is almost uncompressed at any flow rate.

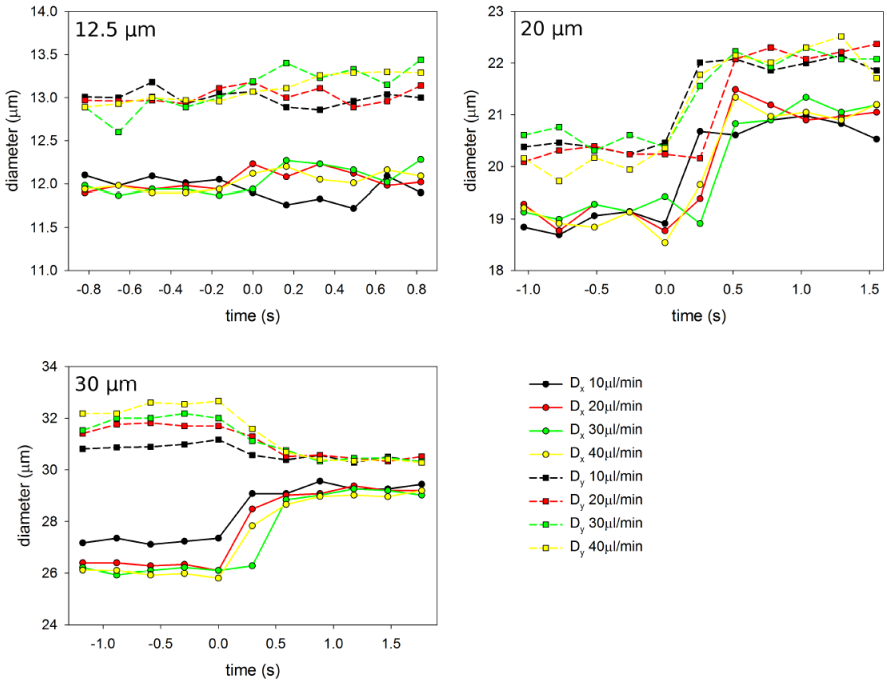

***Figure S6**: Plots of D_x and D_y of GUVs when stopping the flow. Each plot contains measurements of a single GUV, but compressed with different flow rates. Top left: smallest GUV of ca. 12.5 µm average diameter. Top right: medium sized GUV of ca. 20 µm average diameter. Bottom left: largest GUV of ca. 30 µm average diameter. D_x are plotted with straight lines and circles, and D_y with dashed lines and squares. The different colors represent different flow rates. The time axes are defined such that the closing of the valve occurs around 0 s. The first and last shown time points were actually collected about 4 s before/after closing the valve to show that there is no significant change in between. They are plotted directly adjacent to the other time points for a better view of the diagram.*

For the medium sized GUV (20 µm) however a change in shape can be observed. Both D_x and D_y rise significantly after stopping the flow. But one would expect only D_x to rise and D_y to drop. This is here because the GUV shifts its z-position when closing the valve. Therefore a different slice of the GUV is measured which is bigger in both D_x and D_y than the slice which was observed during shear stress. This is not optimal for domain obervations over time, but it can be seen that the transition occurs in under 0.5 s and that there is no significant change in shape afterwards. Different flow rates do not have an impact on the amount of the deformation. The biggest GUV (30 µm) behaves how one would expect. Its D_x increases and its Dy decreases after stopping the flow. Now it can been seen how different flow rates affect the deformation. As one would expect, faster flow rates deform the GUV more, but after stopping the flow the D_x and D_y values all arrive at the same equilibrium. For all GUVs, one

would expect D_x and D_y to be the same after stopping the flow, because the GUVs should be spherical. This is however not the case here. The reason is that in all three examples the GUVs interacted with the traps, making them not completely spherical. As mentioned above, such cases were not evaluated for the domain dynamics experiments. For these deformation experiments this interaction isn't optimal, but one can still see that after stopping the flow, the GUVs only take about 0.5 s to return to their equilibrium shape. This means there is no change in shape observed for the domain-dynamics experiments, which have slower acquisition times than 0.5 s.

6. Analysis of domains over time

The GUVs were scanned in 12 to 16 slices, depending on their size, with a resolution of ca. 3 µm in z-direction (direction of the excitation light) within 10 to 20 s. This time resolution was mostly too slow to observe the initial changes of shapes of the domains but sufficiently fast to monitor the diffusion and fusion of these domains, which occurred over several minutes.

A good measure for domain fusion would be the determination of the domain perimeters, and their changes over time. While it is in principle possible to assess these data from the 3D stacks, it turned out to be not useful in practice. First, because not all domains were round when they fused, which complicated the analysis. Second, because the vesicle often still moved or rotated slightly even when the flow was stopped. Therefore, an alternative approach was used, where the number of domain transitions in the image slices is determined, i.e. the total edge points (TEP). The decrease of the TEP is a means of domain fusion and allows for comparison of the fusion behavior in different GUVs.

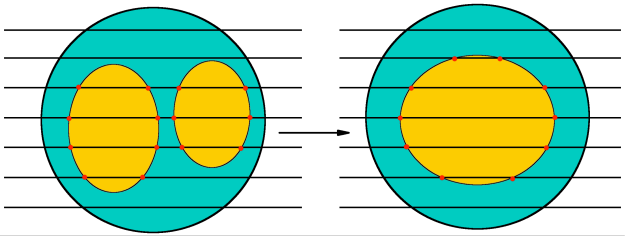

Figure S7. *Schematics of a GUV with two domains that fuse to one larger domain. To analyze the fusion, the GUV is divided in slices and the number of transitions from one to the other domain is counted. This number is referred to as total number of edge points (TEP).*

The edge points were detected with the following procedure. Using the software ImageJ, a

Gaussian blur (sigma=4) was applied to both the DiI and the NAP channel. To each pixel intensity of the DiI channel a value of 100 was added and the NAP was subtracted from the DiI to improve the contrast between l_o and l_d (see Fig. S7). Without adding 100 to the DiI channel, information would get lost with the subtraction because the pixels cannot take values below zero. For each slice a line was traced along the GUV perimeter with a width of ca. 20 pixels (see Fig. S8). A plot of the average pixel intensities along this line was calculated using the function "Plot Profile". This plot now shows high intensity, where the phase is l_d (DiI) and low intensity, where it is l_o (NAP). In Matlab, noise of the plot was reduced with the function "smooth" (span=15). Then a threshold was set between the intensities of l_o and l_d, and each point where the intensity crosses the threshold was counted. These points are the edge points of domains.

This was conducted for each image, the points were summed up over the entire stack, and then plotted against time. For each slice, a separate line was traced along the GUV perimeter, but the same line was used for each time point. This could only be completed if the GUV didn't move in the z-direction during acquisition, otherwise a different line with a new diameter would have had to be drawn for each single frame.

To fit the data a first order kinetic model was used: $A = c + A_0 e^{-kt}$ where t is the time, A is the TEP, A_0 is the difference of TEP between t = 0 and t = ∞, c is the TEP at t = ∞ and k is the rate constant of the signal decay. Because k only depends on the decay rate of the TEP, it is a good measure for the fusion rate of domains and allows comparisons across difference experimental conditions. We chose to only consider measurements which produced rate constants k with a confidence interval smaller than 80%. A typical reason to remove a curve is the movement of the vesicle out of focus, or any unwanted photobleaching. Other possibilities are that the vesicle has no domains, or the contrast was too low or we had some flow in the chamber because the valve did not close properly. We first fitted the data and selected afterwards by checking why the fit was very poor.

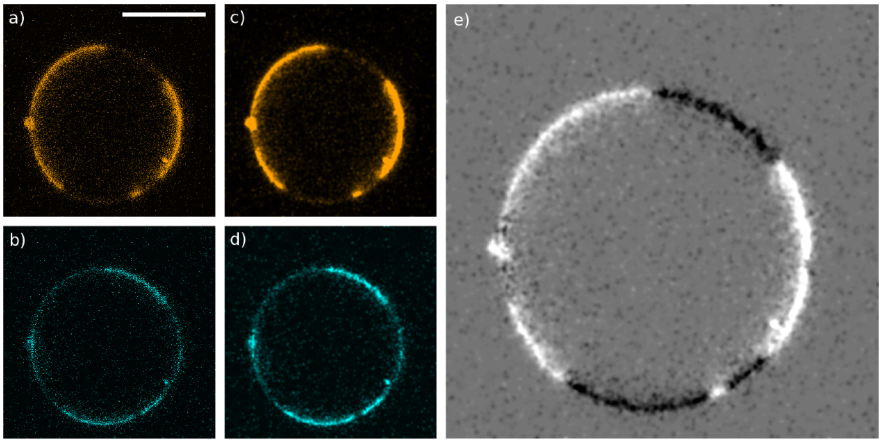

Figure S8. *Example of image processing. The raw data from the DiI (a) and NAP (b) detection channels are processed with a Gaussian blur (c+d). A value of 100 is added to the DiI channel, and the NAP is subtracted (e). Scale bar: 20 µm.*

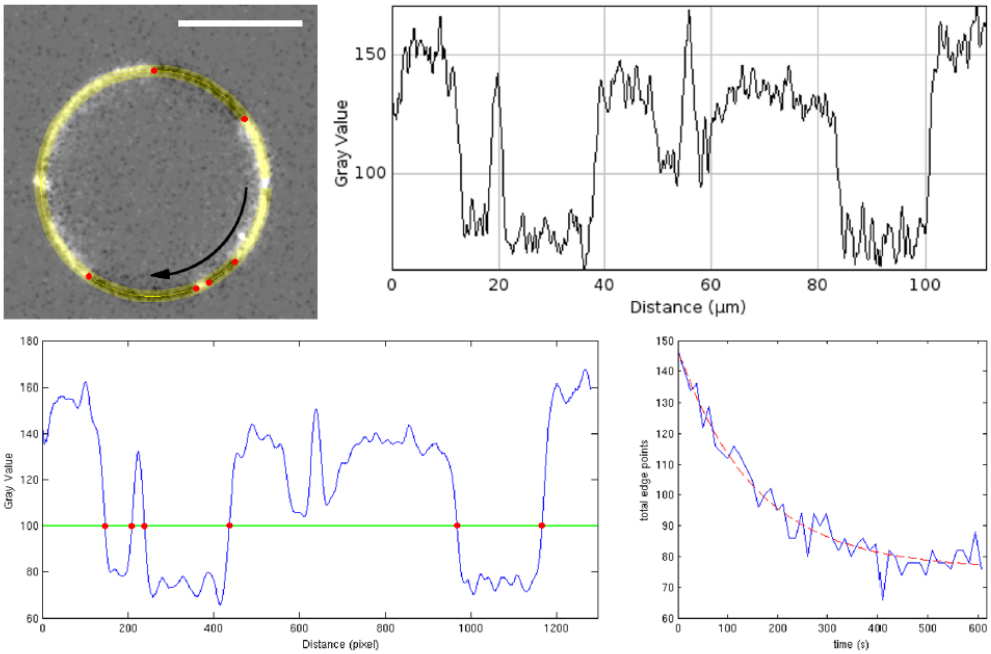

Figure S9. *Example of data collection. Top left: A line (yellow) is traced along the GUV perimeter. The red dots indicate the domain transitions. A profile of the line is plotted in the direction of the arrow (shown in the top right panel). Bottom left: The plot is processed in Matlab and each time the curve crosses a threshold (green line) is counted. These crossings are marked with red dots, which correspond to the ones in the top left panel. Bottom right: The edge points are now counted for every slice, summed up and plotted against time (blue curve). The data is fit with a first order kinetic model (red dashed line).*

7. Budding domains

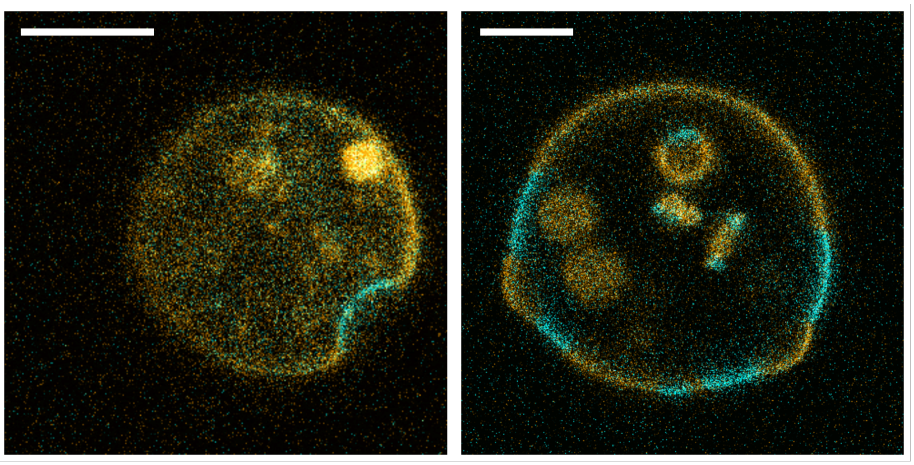

Figure S10. *GUVs with budding domains (SM/DOPC/Chol 0.4:0.4:0.2). Scale bar: 10 µm. It is interesting to note that the GUV in the left panel has an inwardly budded domain as a result of the flow.*

8. Domain growth after arresting flow

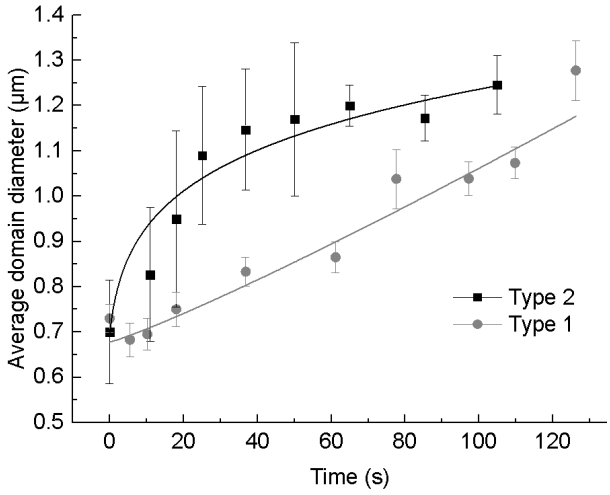

Figure S11. *Domain growth after shear. Confocal slices were recorded at the bottom of the GUVs at 22 °C for up to ~2 min, and the domain diameter was analysed using Zen software (Zeiss). The data was fitted using a power law. For a GUV with the composition of SM/DOPC/Chol 0.52:0.22:0.26 (designated as Type 1) we found the average domain diameter of D(t)) $\sim t^{0.87}$ and for a GUV with the composition SM/DOPC/Chol, 0.4:0.4:0.2), we found D(t) $\sim t^{0.13}$ (here labelled as Type 2).*

9. Calculation of wall shear stress

To calculate the wall shear stress, we implemented the following formula:[5]

$$\text{shear stress} = \text{shear rate} \times \text{dynamic viscosity}.$$

The shear rate given by:

$$\text{shear rate} = \frac{6 \times Q}{w \times d^2}$$

where Q is the flow rate, w is the channel width, and d is the channel depth.

10. Domain tracking analysis

To obtain the movies, data were filtered using a Gaussian blur, then the NAP-channel was subtracted from the DiI-channel for improved contrast. Finally, the images from the top half or bottom half were combined to achieve a projection of a GUV hemisphere. Using these movies, the clearly visible domains were tracked using the software Imaris.

The following results were obtained:

Movie 4: Mean speed of the domains vary from 0.04 – 0.44 μm/s, the longest tracked domain before fusing moves over 39.48 μm and has a mean speed of 0.13 ± 0.11μm/s**.** Average of all domains, excluding the one in the middle that is attached to the wall: 0.14 ± 0.11 μm/s.

Movie 5: Mean speed of the domains vary from 0.06 – 0.19 μm/s, the longest tracked domain moved 100.81 μm with an average speed of 0.13 ± 0.04 μm/s**.** Average speed of all domains were 0.12 ± 0.04 μm/s.

Movie 6: Mean speed of the domains vary from 0.09 –0.16 μm/s, the longest tracked domain moved 65.57 μm/s with an average speed of 0.09 ± 0.05 μm/s**.** Average of all domains were 0.11 ± 0.06 μm/s.

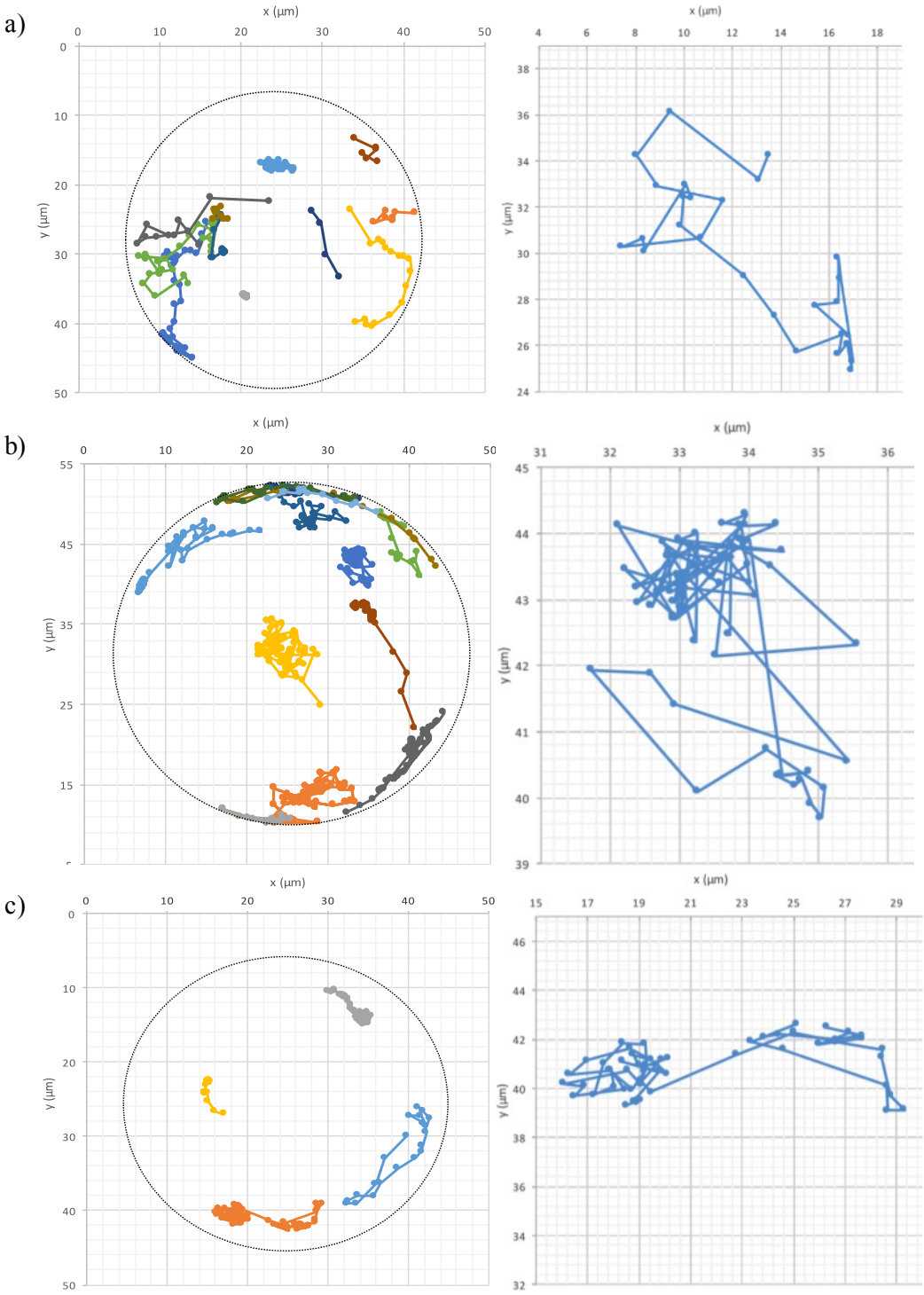

Figure S12. *Tracking plots from a) movie 4, b) movie 5 and c) movie 6. Left: Overview of all tracked domains. Right: An enlargement of a single track.*

References.

1. Angelova, M. I.; Dimitrov, D. S. *Faraday Discuss. Chem. Soc.* **1986**, *81*, 303.

2. Herold, C.; Chwastek, G.; Schwille, P.; Petrov, E. P. *Langmuir* **2012**, *28* 5518–5521.

3. Kuhn, P.; Eyer, K.; Robinson, T.; Schmidt, F. I.; Mercer, J.; Dittrich, P. S. *Integr. Biol.* **2012**, *4*, 1550.

4. Robinson, T.; Kuhn, P.; Eyer, K.; Dittrich, P. S. *Biomicrofluidics* **2013**, *7*, 044105.

5. Coulliette, C and Pozrikidis, C, Journal of Fluid Mechanics,**1998**, 358, 1–28.